Adaptive Visual and Auditory Map Alignment in Barn Owl Superior Colliculus and Its Neuromorphic Implementation

Adaptive Visual and Auditory Map Alignment in Barn Owl Superior Colliculus and Its Neuromorphic Implementation

Juan Huo, Alan Murray, *Fellow, IEEE*, and Dongqing Wei

***Abstract*— Adaptation is one of the most important phenomena in biology. A young barn owl can adapt to imposed environmental changes, such as artificial visual distortion caused by wearing a prism. This adjustment process has been modeled mathematically and the model replicates the sensory map realignment of barn owl superior colliculus (SC) through axonogenesis and synaptogenesis. This allows the biological mechanism to be transferred to an artificial computing system and thereby imbue it with a new form of adaptability to the environment. The model is demonstrated in a real-time robot environment. Results of the experiments are compared with and without prism distortion of vision, and show improved adaptability for the robot. However, the computation speed of the embedded system in the robot is slow. A digital and analog mixed signal very-large-scale integration (VLSI) circuit has been fabricated to implement adaptive sensory pathway changes derived from the SC model at higher speed. VLSI experimental results are consistent with simulation results.**

***Index Terms*— Inhibitory network, spike density calculator, parallel sensory information, spatial localization, spike timing dependent plasticity (STDP), superior colliculus, very-large-scale integration (VLSI), visual and auditory integration, axon growth, e-puck robot.**

I. Introduction

THE AIM of this paper is to bridge between neuroscience and engineering for the adaptive integration of sensory information, using spiking neurons for parallel computation of adaptive sensory systems in the superior colliculus (SC) of a barn owl. Biological experiments show that the juvenile barn owl is able to adapt its localization process to prism wearing, causing a shift of its visual field. The registration between visual and auditory map can be recovered after several weeks' training. The main area of plasticity of map alignment is between the inferior colliculus (IC) auditory map and the SC auditory map, as revealed by anatomical and physiological experiments. It is also the area where the sensory information channels or pathways are changed by the continuous information disparity caused by wearing a prism. This paper introduces a modified mathematical model of the above points based on our previous SC modeling in [1]. The new model is able to carry out adaptive sensory signal integration in a changing environment. It has already been shown in [2] and [3] that this adaptability can reduce the disparity between visual and auditory information. In this paper, the model is further studied and verified by being implemented into a robot demonstrator and then tested in a neuromorphic very-large-scale integration (VLSI) chip.

For this verification, a robot demonstrator, an e-puck robot, provides a hardware body which is analogous to the barn owl head, because it can access sensory stimuli in real time and transmit signals back to a simulation model of an artificial SC. The robot is described in [4]. Experiments in three different scenarios were carried out, in which the experimental results are consistent with simulation results from a mathematical SC model. However, the process is slow. To speed up the computation, a VLSI circuit is designed emulating the SC model in AMS 0.35 μm complementary-metal-oxide-semiconductor (CMOS) process.

Neuromorphic circuits have been designed, aiming for an engineering solution to problems where biological systems currently outperform artificial systems [5]–[9]. A neuromorphic VLSI circuit can be used to compute using neural spikes directly. Thus, the VLSI circuit can provide higher computing speed. In this case, a mixed signal neuromorphic circuit performs a direct hardware level simulation of a mathematical SC model. The results of the on-chip learning are consistent with biological barn owl experiments. Therefore, this circuit can be a solution for a small robot to complete complex computation autonomously, as small robots cannot carry a normal CPU or large microprocessor. The chip presented in Section V is also the first SC model circuit in silicon for adaptive sensory map alignment and sensory information channel adjustment.

II. Map Alignment in the Barn Owl: Biological Background

In neuroscience, the sensory maps in the SC are projected from the other parts of brain, including the retina and IC. Visual stimuli are elicited from the retina and projected to the superficial SC in such a way that only a particular SC neuron responds to visual input from a particular location in space [10], [11].

Manuscript received July 18, 2011; revised May 27, 2012; accepted May 28, 2012. Date of current version August 1, 2012. This work was supported by the Engineering and Physical Sciences Research Council (EPSRC) through the Neuroinformatics Doctoral Training Centre.

J. Huo is with Shanghai Jiaotong University, Shanghai 200240, China, and also with Zhengzhou University, Zhengzhou 450001, China (e-mail:juanhuo@126.com).

A. Murray is with the Institute of Integrated Micro and Nano Systems and Neuroinformatics Doctoral Training Center, University of Edinburgh, Edinburgh EH9 3JL, U.K. (e-mail: Alan.Murray@ed.ac.uk).

D. Wei is with Shanghai Jiaotong University, Shanghai 200240, China (e-mail: dqwei@sjtu.edu.cn).

Color versions of one or more of the figures in this paper are available online at http://ieeexplore.ieee.org.

Digital Object Identifier 10.1109/TNNLS.2012.2204771

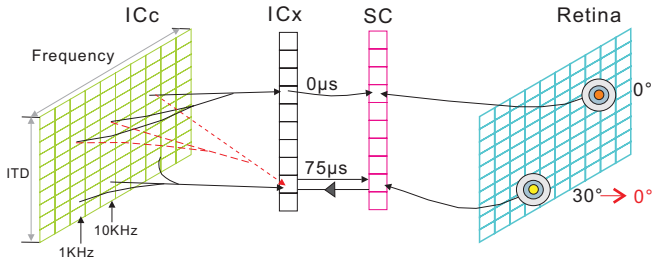

Fig. 1. Audio-visual integration in barn owls. The solid black arrow represents the pathway of sensory information integration in a normal barn owl before wearing a prism. The dashed line between ICc and ICx represents the new axon connection with a prism in place. ITD is mapped in frequency-specific channels in the brain stem. This information ascends to the ICc, and projects from the ICc to the ICx, where a map of space is created. The connections between visual map and the SC do not change. The large triangle sign from SC to ICx near the bottom line is the instructive signal, MAC, generated by the interneuron in the SC. The upper circle of the retina map initially represents 0°. With a prism in place, the upper circle no longer represents 0°. Instead, the lower left circle which was 30° initially is now 0°. This change creates a shift between visual and auditory maps.

The auditory stimuli to the SC come from the external nucleus of IC (ICx), which is a part of IC [3], [12]. The remainder of IC is called the central nucleus of IC (ICc) which takes most of the area of IC. The auditory map in ICc shows phase ambiguity because of the tonotopic organization of ICc neurons as in Fig. 1. In comparison, a neuron in ICx is nontonotopic and responds to a specific position in space. The neural activity in IC is sensitive to the interaural time difference (ITD) between input sound waves of two ears. ITD is an auditory localization cue for the angle of azimuth [13]–[15].

Auditory inputs of similar pitch project to similar regions of the ICc. The information converges during projection from the ICc to ICx and frequency information is lost, because ICc neurons within the same ITD laminae but different frequency response are connected to a single ICx neuron. This means that each neuron in the ICx is sensitive to a specific ITD, namely its "best ITD." The auditory maps formed in the ICx and the ICc also show different sensitivity to changes in the visual map.

The projection of auditory information onto the ICx adapts when the visual map in the SC is shifted, for example, by a prism. It is believed that the SC represents the visual space topographically and thus provides a template for the ICx map shift, but has no effect on ICc. It has been shown that axon sprouting and/or retraction (axonogenesis) and synapse formation/removal (synaptogenesis) are involved in this adaptation [10], [12]. An inhibitory network in the SC modulates the visual signal to allow adaptation only when auditory and visual maps are misaligned. Visual activity does not excite the ICx neurons if visual and auditory localization cues are aligned, but is strong if visual and auditory maps are not in register. Here, the modulated visual signal that triggers adaptation is called the map adaptation cue (MAC). Between the ICc and ICx, the axon growth factor is released to guide the growth of new axon connections. MAC is defined here because it has been shown in biological experiment that postsynaptic action potentials can trigger the release of axon growth factor from the spiking neuron [16] and the contribution for axon growth from intracellular signals is reported in [12]. Although neurotrophin has not been proved to be the main guidance factor in this process, we use it in the following sections to represent the axon growth factor.

In summary, the information stimuli flow from ICx and the retina to bimodal neurons of the SC and adaptation occurs between the ICx and the ICc. The output of the SC multisensory neuron is delivered to the deeper layers of the SC and is connected to the motor system, where the effect of the prism is transferred to the change of orientation behavior [2]. This whole process is shown in Fig. 1.

III. SC Model

Several different models have been suggested for the barn owl SC. [3], [17], [18], and [19] used Hebbian learning mechanisms and neurons in these papers are value dependent. In comparison, [20] explored the integration of visual and auditory inputs using a nonlinear spiking neuron, but without adaptation and plasticity. The role of spike timing dependent plasticity is also discussed in [21], which has a different network strucutre without axonogenesis. The SC model in this paper uses an inhibitory network for the SC bimodal neuron and provides the MAC signal for the IC. This model has a mechanism that can reproduce recent biologically plausible values with respect to adaptation in the presence of a prism.

Fig. 2 shows the neural network. Each pathway represents one direction in azimuth. The angle interval between each pathway is 18°. To analyze its structure more clearly, the first pathway of the network is divided into two blocks. Block I comprises the ICc, ICx, and the axonal connections that map between them. Block II is the controller for the ICx/ICc mapping in Block I. Map adaptation in Block I is initiated and directed by a learning-control signal from an interneuron in Block II. The interneuron in Block II is connected with the SC bimodal neuron through an inhibitory synapse. The arrangement of the interneuron is based on the observation that the visual activity in the ICx is gated by an inhibitory network in SC [22]. The modeled inhibitory synapse between the bimodal neuron and inhibitory neuron results in the modulation of the MAC. In Block II, all the bimodal neurons and interneurons are leaky integrate and fire (LIF) neurons, which are often used in neuromorphic designs [23]–[26]. Although in terms of biological details IF neurons are less realistic than the conductance based ones like Hodgkin-Huxley neuron model, they have fewer parameters and components. This is important if the SC network is to be extended to a larger network in the future, because it means that a VLSI IF model needs fewer transistors and is less complex.

In Fig. 2, neuron N_{ij} indicates the neuron located in layer i and pathway j. The development of axon growth cone is activated by presynaptic spikes from its source layer ICc (layer 1). The target layer ICx (layer 2) releases neurotrophin when it is excited by MAC spikes. The concentration of neurotrophin c_{2j} is set to be linearly proportional to the synaptic activity on neuron N_{2j} which is induced by MAC cues and represented as $M\_spike(N_{2j})$. Among neurons in layer 2, N_{2y} is set as

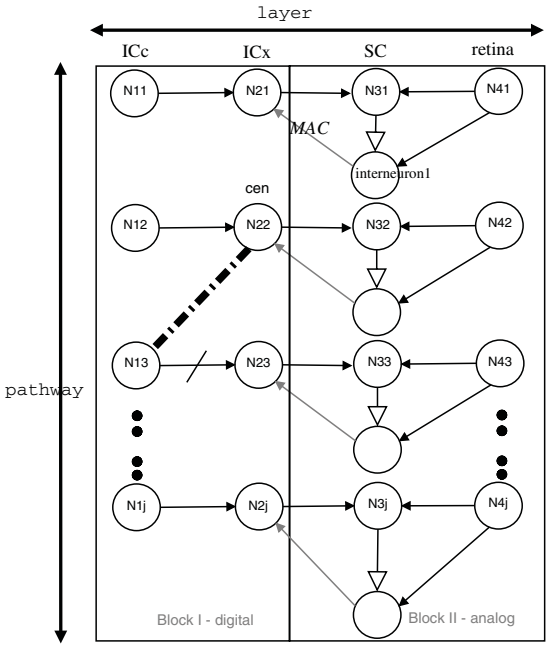

Fig. 2. Modeled network response to visual and auditory misalignment created by a prism. Neurons are shown as circles. The filled arrows represent the excitatory synapses, but the hollow arrow is the inhibitory synapse. The auditory input (A) represents the peak inputs, namely the site in the auditory map that corresponds most closely to the stimulus. The visual stimulus (V) arrives in the retina at N_{42}, and N_{22} receives the strongest MAC. The (misaligned) auditory stimulus arrives at ICc neuron N_{13}, whose axon growth cone is consequently attracted by neurotrophin released by N_{22}. After training, a new connection is made between N_{13} and N_{22}, shown as a dashed line. Although the original connection between N_{13} and N_{23} is still extant, the information path is blocked in the model, by depression of the axonal conductance.

the ICx neuron that receives strongest stimuli from Block II. The concentrations of neurotrophin released by layer 2 neurons depend upon the distance between neuron N_{2j} and N_{2y}. To emulate the extra cellular environment, c_{2j} is contributed by all active release sites; this contribution, however, decays rapidly with distance from N_{2y} and the neighboring neuron's contribution is few in this model. For any position between ICx and ICc, the neurotrophin concentration decreases with time if there is no new release. So c_{2y} can be expressed as

$$c_{2y}(t) = \sum \varepsilon M\_spike(N_{2y}) e^{-\lambda(t)} \tag{1}$$

where ε and λ are constant parameters, and t represents a time step [27]–[29].

In the ICc layer, the growth cone activity G_{1x} is bounded by a presynaptic factor $N\_spike(N_{1x})$, which is a summation filter representing the linear sum of the presynaptic spikes of the corresponding neuron N_{1x}. If the neural spikes stop, G_{1x} decays rapidly with time t. So in equation (2), G_{1x} is

$$G_{1x}(t) = \sum \varepsilon N\_spike(N_{1x}) e^{-\xi(t)} \tag{2}$$

where ξ is another constant parameter to describe time decay. The growth cone on pathway x is activated when G_{1x} is above a certain value, whereupon the connection from neuron N_{1x} has the highest probability to be extended.

The key factors in the adaptation process are c_{2y} and G_{1x}. The information pathway will not be changed until c_{2y} and G_{1x} are all above their thresholds. If N_{2y} is the target direction of the growth cone G_{1x}, the position number of N_{2y}, y, is identified when the accumulated neurotrophin c_{2y} exceeds the neurotrophin concentration threshold, then the new connection between N_{1x} and N_{2y} is validated. Meanwhile the neurotrophin is reset to the initial state. When the new connection is complete, the old connection from the same neuron will be blocked according to [30] and [31]. The model in this paper is a modification from our previous work in [1].

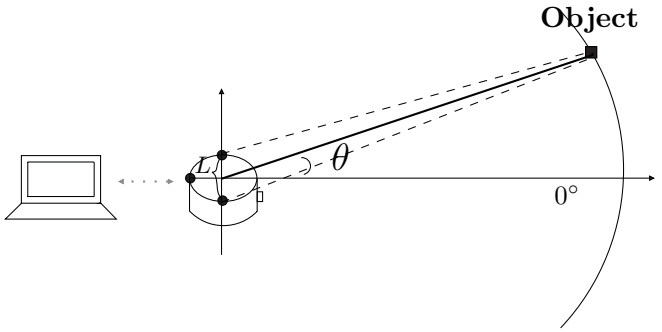

Fig. 3. Experiment environment (schematic). The visual and auditory stimuli sources are located in a semicircular track. The robot is equipped with two microphones and a camera. The robot sends the sensory data to the laptop through Bluetooth in real time.

IV. Barn Owl Robot Demonstrator

We tested this SC model in a robot demonstrator, using an e-puck robot. The e-puck robot with a diameter 70 mm and height 50 mm is built around a Microchip dsPIC microcontroller with 8 KB RAM and 144 KB of flash memory. The robot contains three microphones to capture sound, and a color CMOS camera with a resolution of 640×480 pixels in front [4]. This robot also has extended connectors and an extension board which can be replaced by an application-specific circuit board.

In previous works on visual and auditory information integration, researchers have concentrated on the coordination between different visual and auditory frames, but few have tested the effect of wearing a real prism on visual and auditory integration [3], [19], [32], [33]. In this paper, a real prism is used over the robot camera, replicating the environment setting for a young barn owl [1]. We have explored the capability of the model in a real-time system. The e-puck robot is equipped with three lateral microphones, and a camera. A 33° prism covers the camera, displacing the visual data laterally. The whole configuration is presented in Fig. 3. The e-puck robot communicates with the host computer by Bluetooth. The loudspeaker produces 1 s bursts of 1 kHz sine wave, and each burst lasts 1 s. The sound signal is sampled at 33 kHz and stored in an array. Unlike many previous sound localization experiments [34], [35], we do not use cross correlation. The sound signal is processed by a fast Fourier transform in a time window. When the average amplitude of the input signal is above a chosen threshold, the characteristic frequency $\overline{f}$ is with the highest amplitude in the Fourier series from the left or right signal. This then yields the ITD Δt and

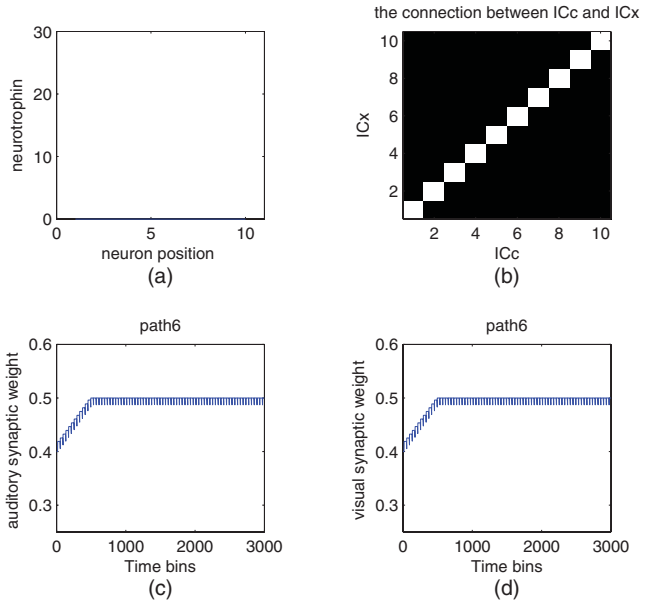

Fig. 4. Visual and auditory localization signals from a same target are registered with one another. (a) No neurotrophin is released by the ICx layer at any time during the experiment. (b) Axon connection between ICc and ICx does not change. (c) and (d) Target direction is in 0°. Both the visual and auditory receptive centers correspond to pathway 6 and their synaptic weights increase simultaneously.

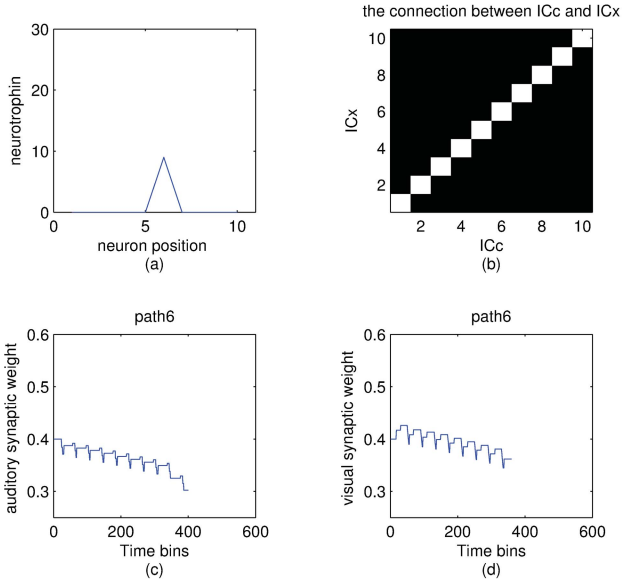

Fig. 5. Visual and auditory localization signals are misaligned. (a) Neurotrophin is released by the target ICx neurons and accumulated. (b) Axon connection between ICc and ICx does not change as the neurotrophin and growth cone do not reach their thresholds. Here the visual receptive center is in pathway 6, while the auditory receptive center is in pathway 8. (c) and (d) Both the visual and auditory synapses are weakened because the input spike trains are independent of one another.

the target azimuth difference θ

$$\Delta t = \frac{\Delta\phi}{2\pi\overline{f}} \tag{3}$$

$$\theta = \arcsin\left(\frac{\Delta t V}{L}\right) \tag{4}$$

where V is the speed of sound in air, L is the diameter of the robot head, and $\Delta\phi$ is the characteristic phase difference between left and right ears.

The robot camera is a normal camera, its visual field is limited to $-30°$ to 30°, so that the camera produces a target image which has 120 pixels in one dimension and each pixel corresponds to 0.5° of a semicircle in the plane. The visual target is a white light-emitting diode (LED), so in the image it is a luminous point. The target point is recognized by identifying the peak value in the image matrix. Because we use a grayscale image, the numerical pixel value ranges from 0 to 255.

The procedure of this experiment has two steps.

1) The owl-head robot was pointed in different azimuthal directions in a random sequence. For every orientation, visual or audio stimuli were presented at one of the ten available locations.
2) The owl-head robot, wearing a prism, was presented to randomly selected azimuthal directions.

For each direction, the target stimulus was repeated 75 times and averaged. Visual and auditory stimuli are generated at the same time but separately from the LEDs and loudspeakers. In the anechoic chamber, the error for the sound localization is very small. The standard deviation of the error in the anechoic chamber is within 1°. In an open environment, the error increases because of echoes and the presence of ambient noise.

A. Results and Robotic Experiment

For step one, at the beginning of the robot experiment, without a prism, visual and auditory objects are aligned. The results for localization of a target at 0° azimuth are shown in Fig. 4. Since visual and auditory signals are registered, both the visual excitatory synapse (the arrow between N_{4j} and N_{3j} in Fig. 2) and auditory excitatory synapse (the arrow between N_{2j} and N_{3j} in Fig. 2) are strengthened. Since visual and auditory input spike trains are highly correlated, the visual synapse of pathway 6 in Fig. 4(c) and the auditory synapse of pathway 6 in Fig. 4(d) increase rapidly to their maximum value of 0.5. This results in a more active bimodal neuron with high firing rate. Because of the inhibitory relationship between the bimodal neuron and the interneuron, the interneuron is strongly inhibited and its firing rate is close to zero, thus very few MAC spikes are generated and no neurotrophin is released by the ICx neuron. This also means $c_{2j} = 0$ as shown in Fig. 4(a). Although the input spike train density in the source layer, ICc, is high enough to activate the growth cone, neurotrophin concentration c_{2j} is far below its threshold, therefore there is no change to the original axon connection, as in Fig. 4(b).

For step two of the experiment, the robot wears a prism over its camera, which means that there is 33° disparity between visual input and auditory input. The luminous light source still comes from a target at 0° while the auditory sound source comes from 33°. The results at different time points are shown in Figs. 5 and 6. In Fig. 5, the prism places the visual receptive center and auditory receptive center in different pathways (pathways 6 and 8, respectively). Visual and auditory input spike trains in pathway 6 are now quite different from each another and are uncorrelated. Both the

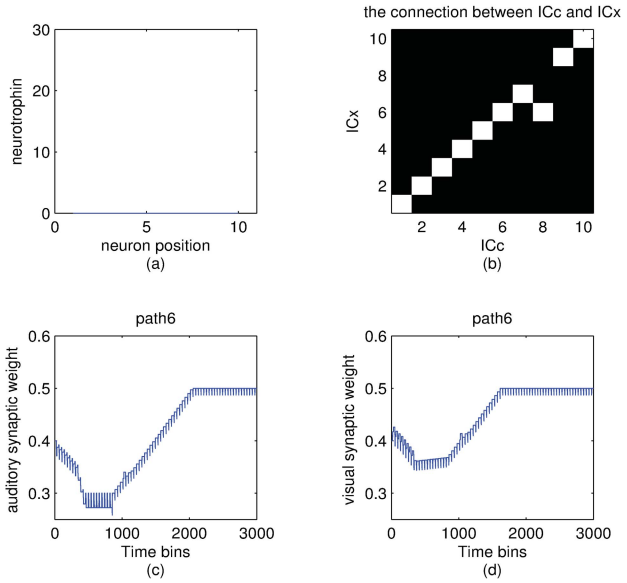

Fig. 6. New axon connection is formed. (a) Axon connection has been updated and the neurotrophin is reset to its original (zero) status. (b) New axon connection is formed and the old connection is inhibited. (c) and (d) Both visual and auditory synapses begin to increase once the visual and auditory signal have been re-registered with one another again.

visual and the auditory synapses connected to the bimodal neuron are weakened. Thus, the SC bimodal neuron in pathway 6 becomes less active and fewer postsynaptic spikes are triggered. As a result, inhibition of the interneuron by the bimodal neuron is decreased and the output spike rate of the interneuron, MAC increases. This stimulates the release of neurotrophin in pathway 6. In the axon source layer ICc, we measure the axon activity by counting the input auditory spike train density. When the accumulated neurotrophin reaches its threshold value (here the value is set 20) in target layer of pathway 6 and growth cone in pathway 8 is ready at the same time, the axon connection network is updated. This also means a new connection between pathway 8 and pathway 6 will be created (the rectangle turns white) and the original connection pathway 8 to pathway 8 is blocked (the rectangle turns black).

The real-time video of this process for the other positions can be seen on the web at http://www.see.ed.ac.uk/~s0454392/research.html.

V. SC VLSI Circuit

Implementation of the SC model in a robot provides a real environment with sensory signal inputs. However, it is merely software. The microcontroller of the e-puck robot has processed the input sensory stimuli indirectly, and its architecture is very different from a neural system, so it requires complex mathematical programming in the PC rather than in the robot which is limited primarily by its memory. The microcontroller dsPIC30F6011A in our robot has only up to 144 KB on-chip Flash program space, thus a connection between the robot and PC is needed.

To make the robot independent, a neuromorphic circuit was designed and fabricated, which is also expected to improve the computing speed and better emulate the biological neural computation. Fig. 7 is a micrograph of this SC chip, in

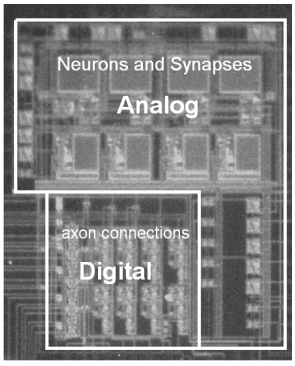

Fig. 7. Micrograph of mixed signal SC chip. The analog block includes four neurons and synapses. The digital block has four switches, registers, and eight spike calculators, although the size of the chip in total is only 0.6 mm × 0.5 mm.

which digital block and analog block sit side by side in just 0.6 mm × 0.5 mm. This chip has four neurons and six synapses and corresponds to the network model in Fig. 8(b). The power supply current is less than 10 mA at 3.3 V. Two information pathways are selected as the basic platform to simulate the visual and auditory integration, whose corresponding network model is shown in Fig. 8(b), which is basically two of the ten pathways in Fig. 2. The system structure was designed to be the same as the neural model and to include an "inhibitory network" and "axon network." The analog part of the circuit is several paralleled "inhibitory networks," which are composed of STDP synapses and LIF neurons. The digital part of the circuit is the axon network, which is composed of switch bars, a status register network and spike counters. The whole mixed signal CMOS chip has been fabricated using a standard AMS 0.35 μm process.

A. Inhibitory Network Circuit

The basic computing units for the analog block are neurons and synapses. The diagram of the circuit components is shown in Fig. 8(a) which represents an inhibitory network in one pathway. The inhibitory network is composed of four different components shown in different colors. The interneuron only accesses visual input and is inhibited by the inhibitory synapse circuit which leaks the current from the IF neuron membrane. Thus, the output firing rate of the interneuron is inversely proportional to the output firing rate of the bimodal neuron. This is also called shunt inhibition in some articles [25], [36], [37]. Shunting is an important type of gain control in biology to regulate neural responses. In this inhibitory VLSI circuit, both interneuron and bimodal neuron are IF neurons, whose circuit is similar to [24]. The circuit of this IF neuron also includes features from [23], [25], and [38]. The parameters of the circuit in Fig. 9 are configured so that the interneuron firing rate is lower than the other IF neuron and its neuron membrane threshold is set to be higher than the other neurons.

Fig. 9(a) is the excitatory synapse based on the simple synaptic structure in SC model. The output current (Isyn), which is connected to IF neuron membrane of the neuron circuit, is controlled by V_w, Vspike, and V_{bias}. Vspike is the train of input spike pulses, which switches on M2 and induces

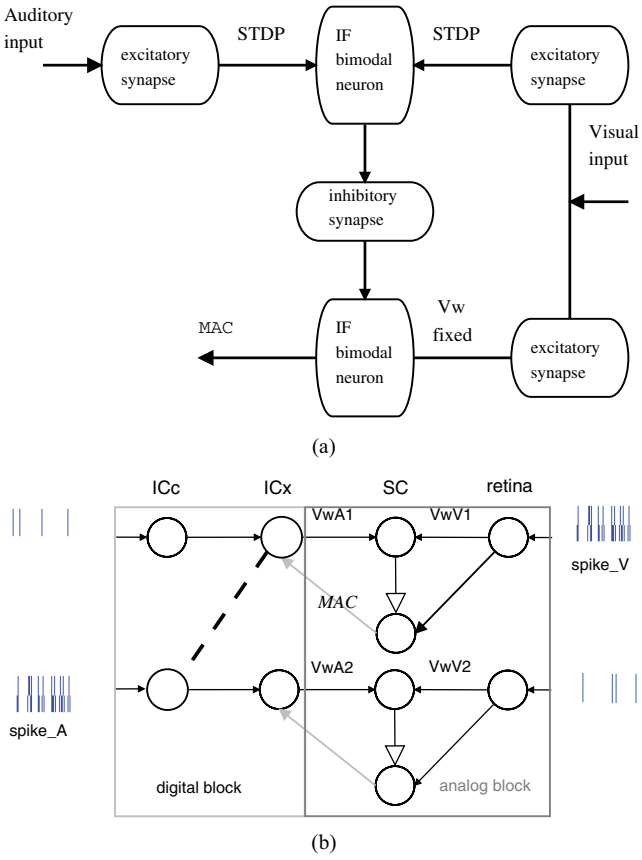

Fig. 8. Inhibitory network block diagram. (a) Electronic synapses connected with the bimodal neuron follow the rule of STDP. Since there is only one synapse connected with the interneuron, its electronic weight value Vw is fixed. (b) This is part of the SC network. Neurons with the same labels are in the same pathway and they are named in the form "layer name - pathway name," for example, ICc-1, retina-1. The synapses connected with the bimodal neurons are also named with their pathway number such as $VwA1$ and $VwA2$. The hollow arrow is the inhibitory connection between the bimodal neuron and interneuron.

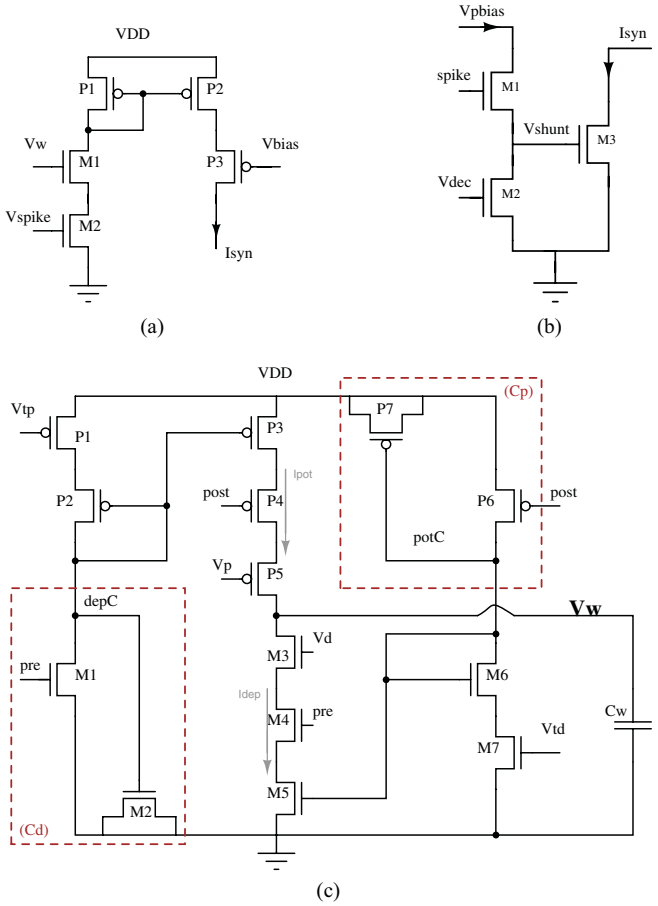

Fig. 9. VLSI synapses used in this circuit. (a) Excitatory synapse. (b) Inhibitory synapse. (c) STDP module dynamically increases or decreases Vw with (causal or anti-causal) co-occurrence of pre- and post-synaptic spikes. Cp and Cd are the two gate capacitors of transistors P7 and M2.

the spike current. Fig. 9(b) is the inhibitory synapse which discharges the membrane current of IF neuron. The interneuron is inhibited by the bimodal IF neuron output, which exerts shunting inhibition on the interneuron. The circuit for shunt inhibition can also be seen in [25], where it is made as simple as merely one conductance. In the circuit shown in Fig. 9(b), the degree of the inhibition is determined by Vpbias and Vdec. By adjusting the Vpbias and Vdec, Vshunt is changed. As a higher voltage value of Vshunt on the transistor gate increases the inhibitory synapse conductance, the inhibitory current which is drawn from the IF neuron is modulated.

Fig. 9(c) is the circuit for modulating excitatory synaptic weights which are represented as VwA and VwV in Fig. 8(b). The excitatory synaptic weight is stored capacitively and is labeled as Vw in Fig. 9. Vw is adjusted by STDP module shown as Fig. 9(c), which is modified from [39]. Two extra MOS capacitors are added in the circuit. Every input presynaptic spike discharges NMOS capacitor M2, which is connected to node depC. During each pre-synaptic spike input, V_{depC} decays immediately and then rises gradually with time. The inverted postsynaptic spike charges the PMOS capacitor P7 and generates V_{potC}. The waveforms of V_{depC} and V_{potC} determine the shape of the STDP learning curve applied to Vw. For each incoming presynaptic spike, the current I_{dep} is controlled by V_{potC}. The current I_{pot}, charging Vw is controlled by V_{depC}. With equal input currents, ΔVw is in inverse proportion to the MOS capacitance, Cp and Cd. In [39], Cp and Cd are only the parasitic capacitance of P6 and M1. The capacitance value is small and varies with CMOS process. Here, the modified Cp is the total capacitance of P6 and P7, Cd is the total capacitance of M1 and M2. Fig. 10(a) shows the resultant RC time constant of depC (approximately 3 ms) with a capacitor area depC of 1 μm^2. The new added two extra MOS capacitors M2 and P7 increase the total capacitance value. Fig. 10(b) shows the effect of increased MOS capacitor area on the RC time constant.

Fig. 11 shows the test results from this inhibitory network, the effect of inhibition on interneuron when the bimodal neuron has higher firing rate. Both SC neuron and interneuron are in the same SC pathway and receiving a high-density input spike train, but their synaptic weights are different: $Vw_{SC} = 2$ V, $Vw_{\text{inter}} = 1.2$ V. The SC neuron has a higher firing rate. The SC neural membrane voltage reaches its firing threshold earlier than the interneuron, so the interneuron is inhibited before its membrane capacitor can accumulate sufficient charge to begin firing.

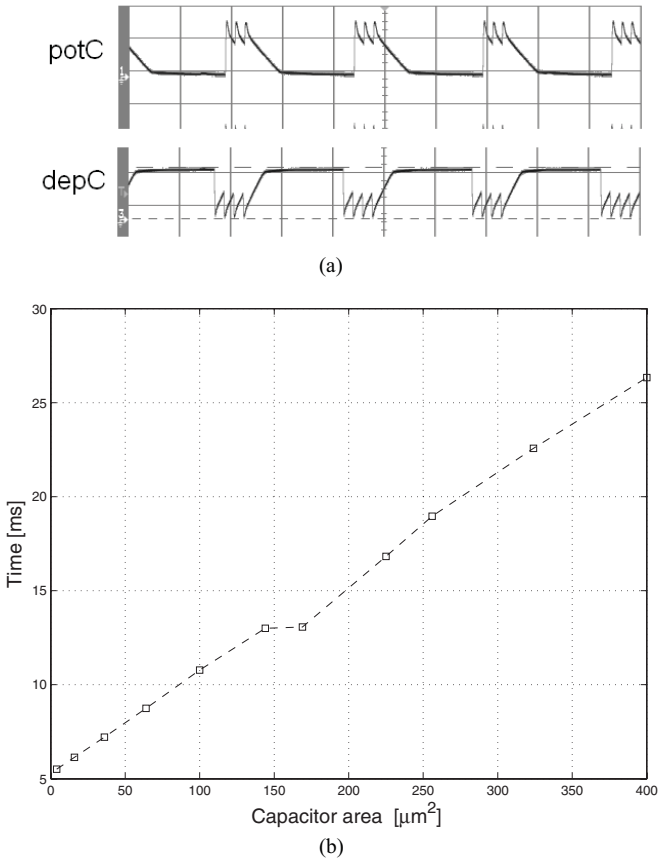

Fig. 10. Effect of synaptic weight change. (a) Curve of depC and potC from the chip with presynaptic and postsynaptic spikes as input. potC and depC are charged and discharged by spikes on switch transistors P6 and M1. The vertical scale of the plot is 2 V/div. (b) Effect of increased capacitor area on time constant of depC.

In the current mirror of Fig. 9(a), the synaptic weight change Vw stored on capacitor Cw of Fig. 9(c) modulates the output current I_{syn}, which is the presynaptic input current that is injected into the membrane of IF neuron circuit. For every input spike, transistor M1 in Fig. 9(a) is turned on if $Vw > V_{TH}$, and in subthreshold if $Vw < V_{TH}$, where V_{TH} is the threshold voltage for MOS device. The firing rate of an IF neuron depends on the input synaptic current, so the relationship between the spike frequencies of the bimodal neuron and the interneuron can be expressed as current-related parameters.

Then we present how the synaptic weight Vw affects the output firing rate. When $Vw > V_{TH}$ and the transistor is in saturation, the synaptic current equation is

$$I_{\text{syn}} = \frac{1}{2}\mu_n C_{ox}\left(\frac{W}{L}\right)(Vw - V_{TH})^2 \tag{5}$$

and for an IF neuron

$$C_{\text{syn}}\frac{\mathrm{d}V_{\text{syn}}}{\mathrm{d}t} = I_{\text{syn}} \tag{6}$$

where V_{syn} is the membrane voltage and t is inversely proportional to the postsynaptic firing rate. So the ratio of the SC neuron firing rate (F_{sc}) and interneuron firing rate (F_{inter}) is given by

$$\frac{F_{sc}}{F_{\text{inter}}} \approx \left(\frac{Vw_{sc}}{Vw_{\text{inter}}}\right)^2. \tag{7}$$

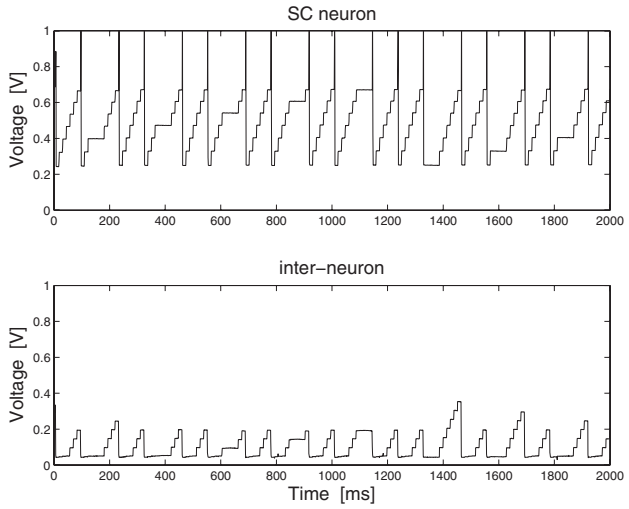

Fig. 11. SC neuron and interneuron firing in an inhibitory network. $Vw_{SC} =$ 2 V, $Vw_{\text{inter}} = 1.2$ V. Although in each SC pathway, the SC neuron and the interneuron share the same visual spike train, the SC neuron fires frequently and the interneuron is inhibited. The inhibitory synapse sinks current from the interneuron more frequently and thus prevents it from firing.

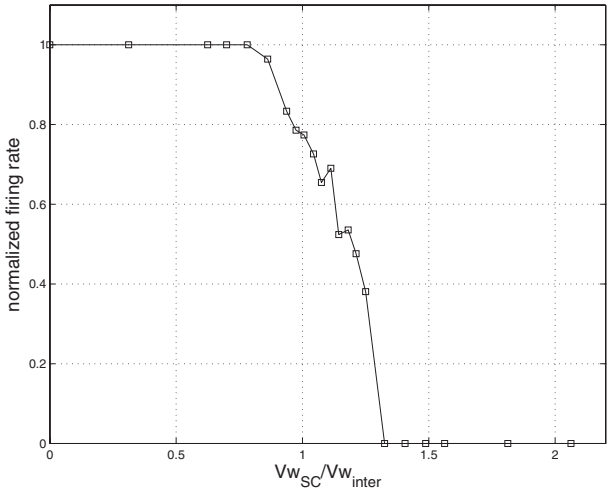

Fig. 12. Variation of normalized neuron firing activity of the interneuron with the weight ratio between the SC excitatory synapse and interneuron excitatory synapses. The interneuron is highly inhibited when this ratio is above 1.5.

To verify equation (7) from the chip, the interneuron synaptic weight value is fixed at 1.6 V. The interneuron synapse works in saturation and the SC excitatory synaptic weight is adjusted between 0 and 3.3 V. The interneuron and SC neuron have the same input spike train firing rate for all the tests. Simulation results shown in Fig. 12 can be explained by the Nyquist–Shannon–Kotelnikov sampling theory: if $(F_{sc}/F_{\text{inter}}) > 2$, namely $(Vw_{sc}/Vw_{\text{inter}}) > \sqrt{2}$, all interneuron spikes will be inhibited by the SC neuron which has high firing rate; if $(F_{sc}/F_{\text{inter}}) < 2$, namely, $(Vw_{sc}/Vw_{\text{inter}}) < \sqrt{2}$, the interneuron firing rate F_{inter} increases as the SC synaptic weight decreases, which is consistent with equation (7).

When $Vw < V_{TH}$, then M1 in Fig. 9(a) is switched off and works in subthreshold. The subthreshold current can be expressed as

$$I_{\text{syn}} = I_o \exp\left(\frac{Vw}{\zeta V_T}\right) \tag{8}$$

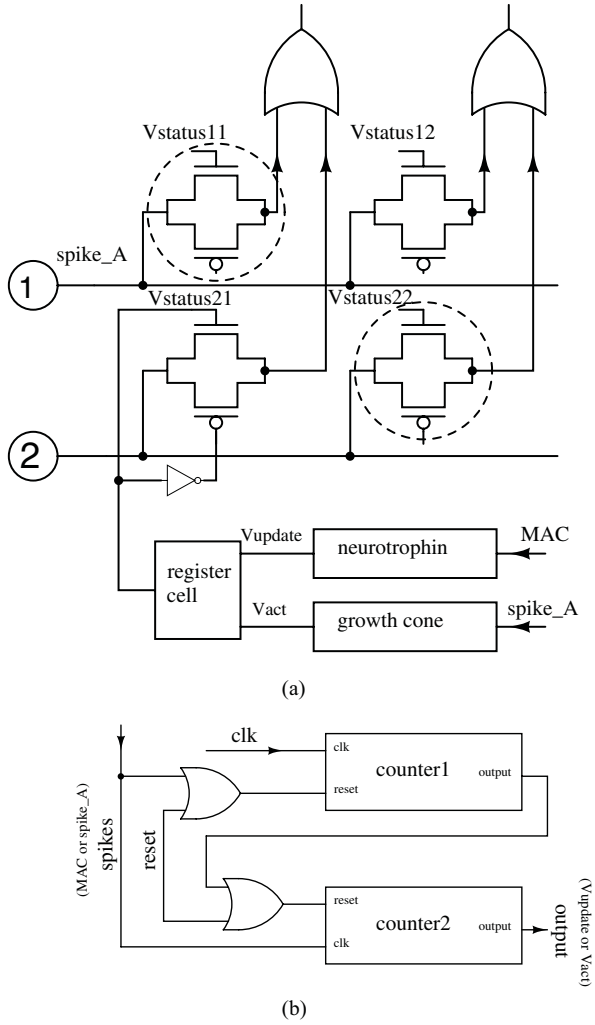

Fig. 13. Digital axon circuit for single pathway block I. The pathways are labeled as circles with numbers 1 and 2. The horizontal labels are input signals and the vertical labels are outputs. (a) Axon connection circuit. OR gates are used between the transmission gates and the IF neurons to merge the spike inputs. The switches which are initially switched on are marked by dashed circles. (b) Spike calculator for the neurotrophin block and growth cone block. It is composed of two counters and two OR gates. The spikes are either MAC from the interneuron or presynaptic spikes of spike_A from the growth cone, respectively.

where $\zeta > 1$ is a nonideality factor and $V_T = kT/q$, k is Boltzman's constant, T is temperature in kelvins, and q is the charge of an electron [40], [41]. The ratio of firing rates is then given by

$$\frac{F_{sc}}{F_{\text{inter}}} = \exp\left(\frac{Vw_{sc} - Vw_{\text{inter}}}{\zeta V_T}\right). \tag{9}$$

This indicates that in subthreshold, the interneuron firing rate also increases as Vw_{sc} decreases. During simulation and chip test, the synaptic output current actually becomes too small to trigger the IF neuron to fire with the required frequency. If the input spike rate is very high and the current leakage is small, the interneuron can fire postsynaptic spikes, but the window of voltage range for $(Vw_{sc}/Vw_{\text{inter}})$ to modulate the postsynaptic spike frequency is narrow, because both

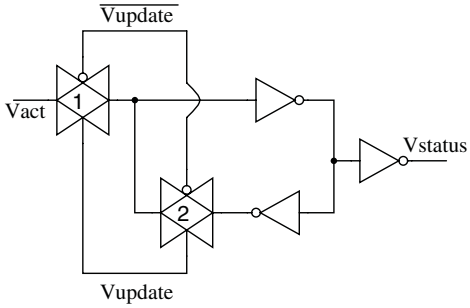

Fig. 14. Circuit of register cell. In contrast to the basic latch (symbols in gray), transmission gates 1 and 2 are added in the feedback loop. This is to avoid any conflict between the input and the feedback. Vact and Vupdate are output signals from spike calculators in Fig. 13. Vact high means the growth cone is active. Vupdate represents an enable signal for the update of network connection.

Vw_{sc} and Vw_{inter} are less than V_{TH}. This can be seen from

$$\frac{F_{sc}}{F_{\text{inter}}} > 2 \Longrightarrow Vw_{sc} > Vw_{\text{inter}} + \zeta V_T \ln 2 \tag{10}$$

where $\zeta V_T \ln 2$ is around 40 mV.

B. Digital Axon Network

The axon network is represented by a digital circuit. It includes three kind of components: crossbar switch, spike calculator, and register.

Fig. 13(a) shows the crossbar switch of axon connections between neurons. Each switch is a transmission gate, a parallel combination of an NMOS and a PMOS transistor. These switches are controlled by signal Vstatus. The value of Vstatus is binary and stored in a register. Each switch status, Vstatus11, Vstatus22, Vstatus12, and Vstatus21, has its own register cell. This reduces the chip area of axons compared with that of capacitors for axon state storage which was used, for example, in [25] and [27]. If the axon circuit expects long time state storage, the capacitor must be expanded in size, however, the larger the capacitor size, the smaller the number of axons we can have within certain chip area.

Switches in Fig. 13(a) can effectively isolate the output from the input and conduct the current in either direction. Output spikes from the switch transmission gates in Fig. 13(a) are sent to an OR gate before they arrive at the IF neuron. The OR gate here also works as a buffer. Transmission gate 1 is used as a switch to update the Vstatus output from register. As shown in Fig. 14, the fundamental storage element of the register is a simple latch. Vact high indicates that the virtual growth cone in the circuit is active. Vupdate represents the neurotrophin update signal. When Vupdate is high, the register updates its state and reads Vact. The conflict between Vact and feedback of the latch is avoided by adding transmission gate 2. Vstatus updates its value upon the rising edge of Vact $\wedge$ Vupdate.

In Fig. 13(a), Vact is asserted by a spike calculator for growth cone while Vupdate is asserted by a spike calculator for neurotrophin. Fig. 13(b) is the spike calculator, which is used to estimate whether or not a spike cluster has arrived in the input. The spike calculator counts the number of spikes and the time interval in a spike train. A spike calculator is composed of toggle flip-flop counters as shown in Fig. 13(b).

Counter 1 counts clock pulses "clk," which is from a regular external clock signal. It is used to estimate the time interval. Each clk adds 1 to counter 1 until it reaches 7. When a new spike comes, counter 1 is reset to 0 and counter 2 counts the number of input spikes. For both counters, the output is high after seven pulses. Counter 2 will not start counting unless the time interval between two spikes is small. If the time delay between two spikes is long, counter 1 will simply count the clk signal continuously.

During chip test, the reset signal is turned off at first to initialize the digital block in Fig. 7. This enables the (3-bit) counter 1 to count external clock pulses. When counter 1 reaches its threshold value, it resets the toggle flip-flop of both counters 1 and 2. Counter 2 sums the input spike train and generates an update pulse when it reaches its maximum value. For the spike calculator of the growth cone, if the output of counter 2 is high, the growth cone is activated. In Fig. 13(a), the spike calculator for the growth cone counts the auditory input spikes in the ICc layer and generates output Vact. The input clk frequency for this counter is 333 Hz, thus the period of each clock pulse is 3 ms. If time interval between two spikes is more than 24 ms, a reset signal for counter 2 will be sent from counter 1. The spike calculator for neurotrophin counts the MAC spikes of the interneuron and generates Vupdate. The input clk frequency for this counter is 6 Hz. If counter 2 of neurotrophin calculator is silent for more than 1.3 s and no new MAC spike appears, the accumulated spike number in counter 2 will be cleared. This is a small deviation from the behavior of the growth cone G_{1j} of equation (2) and neurotrophin concentration c_{2j} of equation (1) in Section III, which gradually decay with time. When the system finishes updating, all counters are reset to their initial state.

C. Input Spike Train Generation

In biology, sensory stimuli induce spikes in clusters, therefore in this simulation, spikes are clustered. The firing rate of neighboring neurons is a random sequence with a low average density. Repeated stimuli are generated from the same position in space to shorten the training time. Differences in spike timing carry information about the location of objects in the environment [42]. Two methods were used to generate spike trains: inhomogeneous Poisson spike trains and spike patterns. The instant firing rate of the center stimulus that induces spike trains spike_A and spike_V in Fig. 8(b), was generated by the following equations

$$r(t) = R\max \times \cos\left(\frac{2\pi t}{T}\right) \tag{11}$$

$$k(t) = \begin{cases} r(t), & r(t) > 0 \\ 0, & r(t) <= 0 \end{cases} \tag{12}$$

where $T = 30$ ms is the period and the maximum firing rate $R\max = 400$ is a constant. $k(t)$ is the inhomogeneous spike firing rate, which varies with time. The rising and falling sections of the cosine function cause the density of this spike train to vary with time and produces regular spike clusters.

For the spike pattern, the time interval between spikes was set according to the choice of the two follows: 1) a high firing rate spike pattern represents the direction of the stimuli in the visual or auditory map center and 2) a low firing rate pattern corresponds to the neurons that are neighbors of the center. The high firing rate spike pattern and the low firing rate spike pattern are independent of each other. The time interval between spikes varies with pattern while the time interval between clusters is a fixed value.

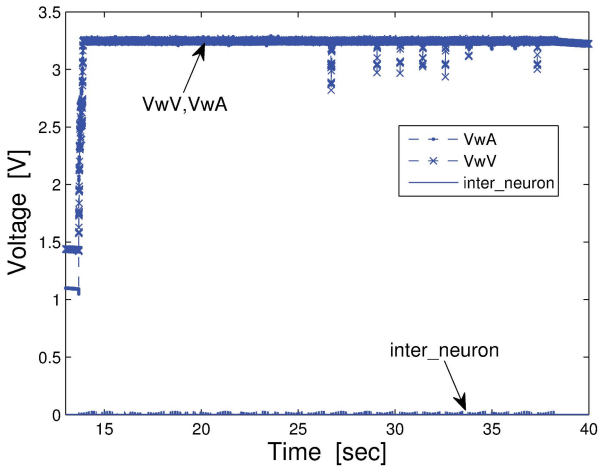

Fig. 15. SC chip test results when the visual input and auditory input spike trains are registered with each other. Data were recorded after synaptic weight initialization finished at 13 s.

D. Adaptation

In the initial status, all the synaptic weight values are set to be 1.5 V, and the switches 1-1 and 2-2 are initially switched on while switches 1-2 and 2-1 are switched off in Fig. 15.

To emulate the prism-free condition, visual input and auditory input are in the same pathway. This setting is similar to the robotic experiment of step (1) in Section IV-A, where the visual and auditory input spike trains are registered with each other. Both the visual and auditory synaptic weights increased quickly from around 1.5 V to 3.3 V at the start of this test, but the interneuron synaptic weight is in a fixed value around 1.5 V. As described in Section V-A, $(Vw_{SC}/Vw_{\text{inter}}) > 2$, the SC neuron output firing rate is much higher than the interneuron, so the interneuron is strongly inhibited and no MAC spikes are out from interneuron. All switch statuses in this case remain unchanged, which represents unchanged axon connections.

To emulate the "with prism" condition, in Fig. 16, the initial status of the switches are still 1-1 and 2-2, but the input stimuli centers are moved to a different pathways such as the visual stimulus is in pathway 1 while the auditory stimulus is in pathway 2 as shown in Fig. 8(b). The synaptic weight at the start of the test is also set to 1.5 V. The initial status values are Vstatus11 = Vstatus22 = 3.3 V and Vstatus12 = Vstatus21 = 0 V. Following the robotic test results in Section IV-A, Fig. 16(a) shows the prism-induced disparity between visual input and auditory input causing a decrease in synaptic weight during the first 26 s. This decreased synaptic weight make the inhibition of the interneuron weaker.

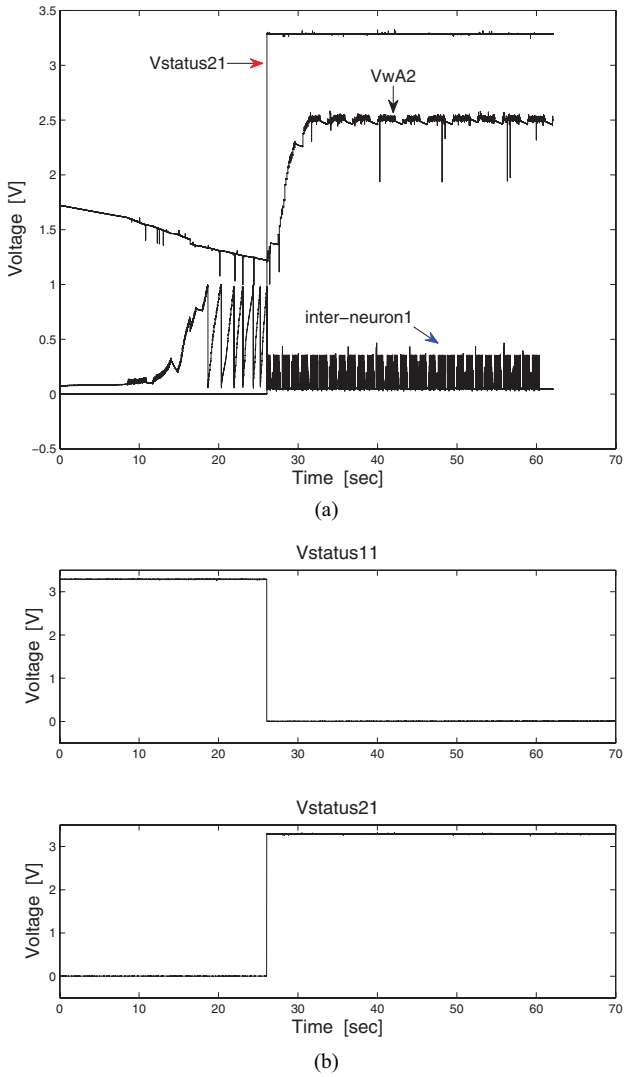

Fig. 16. SC chip test results when the signal pathway is changing. Labels in this figure correspond to those in Fig. 8. (a) VwA2 gradually decreases first but starts to increase when Vstatus21 is on. At the bottom of the figure is the membrane voltage of interneuron1. Before the change of Vstatus21, interneuron1 is active with high-density input spike trains. The switch status changes on the time of the seventh interneuron postsynaptic spike. (b) Vstatus21 is turned on and the new connection between pathway 1 and pathway 2 emerges, but Vstatus11 is turned off.

This decrease ends when the switch status changes at the time shown in Fig. 16(b), recorded from the digital block. Vstatus11 represents the status of the switch on the path 1-1 and Vstatus21 corresponds to path 2-1 in Fig. 13. The falling edge of Vstatus11 turns the switch in path 1-1 off, while the rising edge of Vstatus21 turns the switch of path 2-1 on. These changes occur immediately after the seventh interneuron postsynaptic spike and are updated by the same signal Vupdate1. At the time of this change, the neurotrophin calculator in pathway 1 receives a MAC spike cluster and the update signal Vupdate1 is turned on to become 3.3 V, while Vstatus11 = Vact1 $\wedge$ Vupdate1, Vstatus21 = Vact2 $\wedge$ Vupdate1. The growth cone 1 is inactive, and Vact1 = 0 V while growth cone 2 is active thus Vact2 = 3.3 V. The newly-formed connection 2-1 re-registers the center of the auditory and (prism-shifted) visual stimuli with one another.

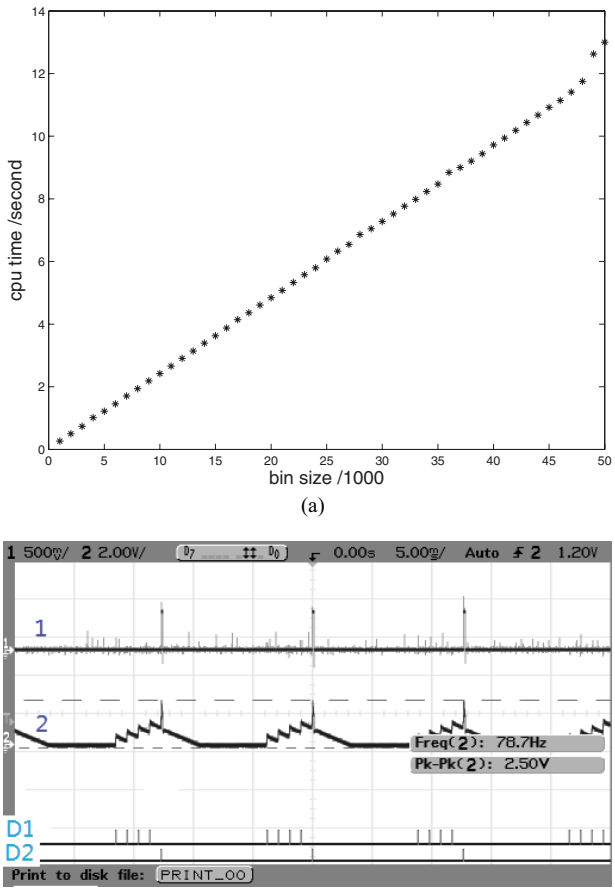

Fig. 17. (a) Time cost of MATLAB simulation from the input to the output is linear. (b) Snapshot of neuron response of the SC chip. D1 and D2 are the input spikes for digital block. Signal 1 and 2 are recorded from analog IF neuron output. During recording, the time scale is 5 ms/div. The time delay between spike input and the resultant output is less than 1 ms.

VI. DISCUSSION

Real-time robot experiments need high computing speed. However, the limited memory storage of the microcontroller and serial port communication used for programming generally cannot satisfy this requirement. During the test of e-puck robot, after the start of sound burst, the time delay from the environmental stimuli and the synaptic weight change in MATLAB was close to 0.7 s.

There is also time cost for computation in simulation. As MATLAB calculates with a whole matrix, we cannot have neural response data after an input spike until 46.9 ms in our simulation. The time cost of MATLAB simulation increases linearly with the matrix size of the spike train. This can be seen from Fig. 17(a). In comparison, the time delay for the SC chip to respond to the input spike is less than 1 ms scale from Fig. 17(b). There is no meaningful time delay between the input spikes and the resulting synaptic weight changes and the sensory spikes are effectively processed continuously. As with other analog neuromorphic circuits, the small number of transistors used also results in a compact hardware package.

The present design has some room for improvement: 1) there is an unstable flip-flop in digital network occasionally,

and the logic components could be improved and 2) the STDP circuit operates in subthreshold mode and will be influenced by parameters such as temperature and transistor mismatch. Identical spike train inputs may therefore result in different synaptic weight bifurcation. Alternative STDP circuits may solve these problems [23]. Furthermore, the synaptic weight capacitor in STDP could be replaced by a floating gate.

VII. Conclusion

Adaptation is a key feature that makes neural networks, in the brain and in artificial systems, interesting, useful, and distinct from conventional computer programs. Although adaptation is a general concept, which is pervasive and is unlikely to have a single theoretical framework, here in this article, we concentrate on sensory adaptation in the midbrain, which can adjust a neural network to the visual and auditory information asymmetric caused by a changed environment. The adaptability of SC in the barn owl can be modeled to allow its central mechanisms to be transferred to an artificial computing system and thereby imbue it with a new form of adaptability to its environment.

A modified computational model of SC has been demonstrated in this paper with reconfigurable axon connections between the visual and auditory maps. The SC model is not only biologically plausible, but also can be used to do more exploration in sensory integration and adaptive neural networks. Real-time processing of detailed sensory information is a computationally demanding task for both biological and artificial systems. Implementation of the SC in a robot is a step toward filling the gap between robots and natural creatures in terms of robustness and flexibility. Neuromorphic VLSI SC is a further step to demonstrate axon rewiring in silicon, processing, and adapting to data without explicit supervision.

Simulation results, robotic experiment, and a VLSI implementation all have proved that the SC model is capable of adaptation similar to that in the biological SC. The adaptation here between visual and auditory maps can be extended to model the integration of other sensory inputs. This paper is a new example of a bio-inspired neural network which can be applied to hardware and provides a new form of self-adaptation in silicon. In addition, it shows that computation based on STDP, as an example of synaptogenesis and axonogenesis, can affect the way in which sensory information transmits between different neural areas.

Acknowledgment

We thank EPSRC for financial support through the Neuroinformatics Doctoral Training Centre. We also would like to thank Martin Reekie and Katherine Cameron for their advice and assistance, and Prof. Feng Zhang's support for chip test equipment.

References

[1] J. Huo and A. Murray, "The adaptation of visual and auditory integration in the barn owl superior colliculus with spike timing dependent plasticity," *Neural Netw.*, vol. 7, no. 22, pp. 913–21, Sep. 2009.

[2] E. Knudsen, "Instructed learning in the auditory localization pathway of the barn owl," *Nature*, vol. 417, no. 6886, pp. 322–328, May 2002.

[3] M. Rucci, G. Tononi, and G. M. Edelman, "Registration of neural maps through value-dependent learning: Modeling the alignment of auditory and visual maps in the barn owl's optic tectum," *J. Neurosci.*, vol. 17, no. 1, pp. 334–52, Jan. 1997.

[4] F. Mondada, M. Bonani, X. Raemy, J. Pugh, C. Cianci, A. Klaptocz, S. Magnenat, J.-C. Zufferey, D. Floreano, and A. Martinoli, "The e-puck, a robot designed for education in engineering," in *Proc. 9th Conf. Auton. Robot Syst. Competit.*, vol. 1. Castelo Branco, Portugal, May 2009, pp. 59–65.

[5] S. A. Bamford, A. F. Murray, and D. J. Willshaw, "Large developing receptive fields using a distributed and locally reprogrammable address-event receiver," *IEEE Trans. Neural Netw.*, vol. 21, no. 2, pp. 286–304, Feb. 2010.

[6] H. Chen, S. Saïghi, L. Buhry, and S. Renaud, "Real-time simulation of biologically realistic stochastic neurons in VLSI," *IEEE Trans. Neural Netw.*, vol. 21, no. 9, pp. 1511–1517, Sep. 2010.

[7] L. Smith and A. Hamilton, *Neuromorphic Systems: Engineering Silicon from Neurobiology*. London, U.K.: World Scientific, 1998.

[8] W. Maass and C. M. Bishop, *Pulsed Neural Networks*. Cambridge, MA: MIT Press, 2001.

[9] Z. Yang, A. Murray, F. Wörgötter, and K. Cameron, "A neuromorphic depth-from-motion vision model with STDP adaptation," *IEEE Trans. Neural Netw.*, vol. 17, no. 2, pp. 482–495, Mar. 2006.

[10] B. Platt, E. Roloff, D. Withington, E. Macphail, and G. Riedel, "Analysis of the superior colliculus auditory space map function in guinea pig behavior," *Neurosci. Res. Commun.*, vol. 23, no. 1, pp. 32–40, 1998.

[11] M. F. Bear, B. W. Connors, and M. A. Paradiso, *Neuroscience: Exploring the Brain*. Baltimore, MD: Lippincott Williams & Wilkins, 2001.

[12] J. Gold and E. Knudsen, "Adaptive adjustment of connectivity in the inferior colliculus revealed by focal pharmacological inactivation," *J. Neurophysiol.*, vol. 85, no. 4, pp. 1575–84, 2001.

[13] T. T. Takahashi, A. D. S. Bala, M. W. Spitzer, D. R. Euston, M. L. Spezio, and C. H. Keller, "The synthesis and use of the owl's auditory space map," *Biol. Cybern.*, vol. 89, no. 5, pp. 378–387, Jan. 2003.

[14] T. Takahashi and M. Konishi, "Selectivity for interaural time difference in the owl's midbrain," *J. Neurosci.*, vol. 6, no. 12, pp. 3413–3422, Dec. 1986.

[15] C. Carr and M. Konishi, "Axonal delay lines for time measurement in the owl's brainstem," *Proc. Nat. Acad. Sci. United States Amer.*, vol. 85, no. 21, pp. 8311–8315, Nov. 1988.

[16] E. Huang and L. Reichardt, "Neurotrophins: Roles in neuronal development and function," *Nature Rev. Neurosci.*, vol. 24, pp. 677–736, Mar. 2001.

[17] J. Gelfand, J. Pearson, C. Spence, and W. Sullivan, "Multisensor integration in biological systems," in *Proc. IEEE Int. Symp. Intell. Control*, vol. 3. Arlington, VA, Aug. 1988, pp. 147–153.

[18] T. Strösslin, C. Krebser, A. Arleo, and W. Gerstner, "Combining multimodal sensory input for spatial learning," in *Proc. Int. Conf. Artif. Neural Netw.*, Madrid, Spain, Aug. 2002, pp. 87–92.

[19] H.-M. R. Arnoldi, "Development of a coordinate transformation for the superior colliculus," M.S. thesis, Diplom-Informatiker, Technische Univ. München, Munich, Germany, 1990.

[20] C. Schauer and H.-M. Gross, "Design and optimization of amari neural fields for early auditory-visual integration," in *Proc. IEEE Int. Joint Conf. Neural Netw.*, vol. 4. Budapest, Hungary, Jul. 2004, pp. 2523–2528.

[21] S. P. Mysore and S. R. Quartz, "Modeling structural plasticity in the barn owl auditory localization system with a spike-time dependent Hebbian learning rule," in *Proc. IEEE Int. Joint Conf. Neural Netw.*, vol. 5. Montreal, QC, Canada, Jul. 2005, pp. 2766–2771.

[22] Y. Gutfreund, W. Zheng, and E. I. Knudsen, "Gated visual input to the central auditory system," *Science*, vol. 297, pp. 1556–1559, Aug. 2002.

[23] A. Bofill-I-Petit and A. Murray, "Synchrony detection and amplification by silicon neurons with STDP synapses," *IEEE Trans. Neural Netw.*, vol. 15, no. 5, pp. 1296–1304, Sep. 2004.

[24] J. Huo and A. Murray, "The role of membrane threshold and rate in STDP silicon neuron circuit simulation," in *Proc. 15th Int. Conf. Artif. Neural Netw.: Formal Models Appl.*, vol. 2. 2005, pp. 1009–1014.

[25] C. Mead, *Analog VLSI and Neural Systems*. Reading, MA: Addison-Wesley, 1989.

[26] G. Indiveri. (2008). *Silicon Neurons* [Online]. Available: http://www.scholarpedia.org/wiki/index.php?title=Silicon_neurons&redirect=no

[27] B. Taba and K. Boahen, "Silicon growth cones map silicon retina," in *Advances in Neural Information Processing System*, vol. 18, Y. Weiss, B. Schölkopf, and J. Platt, Eds. Cambridge, MA: MIT Press, 2006, pp. 1329–1336.
[28] G. J. Goodhill, "A theoretical model of axon guidance by the robo code," *Neural Comput.*, vol. 15, no. 3, pp. 549–564, Mar. 2003.
[29] T. M. Gomez, E. Robles, M. M. Poo, and N. C. Spitzer, "Filopodial calcium transients promote substrate-dependent growth cone turning," *Science*, vol. 291, no. 5510, pp. 1983–1987, Mar. 2001.
[30] E. W. Dent and F. B. Gertler, "Cytoskeletal dynamics and transport in growth cone mobility and axon guidance," *Neuron*, vol. 40, no. 2, pp. 209–227, Oct. 2003.
[31] H. Hatt and D. O. Smith, "Synaptic depression related to presynaptic axon conduction block," *J. Physiol.*, vol. 259, no. 2, pp. 367–93, Jul. 1976.
[32] H. G. Okuno, K. Nakadai, T. Lourens, and H. Kitano, "Sound and visual tracking for humanoid robot," *Appl. Intell.*, vol. 20, no. 3, pp. 253–266, May 2004.
[33] C. Schauer and H. Gross, "A computational model of early auditory-visual integration," in *Proc. 25th DAGM Symp. Pattern Recognit.*, vol. 2781. 2003, pp. 362—369.
[34] M. Rucci, J. Wray, and G. Edelman, "Robust localization of auditory and visual targets in a robotic barn owl," *Robot. Auton. Syst.*, vol. 30, nos. 1–2, pp. 181–193, Jan. 2000.
[35] J. Murray, S. Wermeter, and H. Erwin, "Auditory robotic tracking of sound sources using hybrid cross-correlation and recurrent networks," in *Proc. IEEE/RSJ Int. Conf. Intell. Robots Syst.*, Aug. 2005, pp. 3554–3559.
[36] A. Bermak and A. Bouzerdoum, "A mixed mode real-time VLSI implementation of a shunting inhibition cellular neural network," in *Proc. IEEE Workshop Signal Process. Syst.*, Lafayette, LA, Oct. 2000, pp. 715–723.
[37] L. Abbott and P. Dayan, *Theoretical Neuroscience*. Cambridge, MA: MIT Press, 2001.
[38] S.-C. Liu and R. Douglas, "Temporal coding in a silicon network of integrate-and-fire neurons," *IEEE Trans. Neural Netw.*, vol. 15, no. 5, pp. 1305–1314, Sep. 2004.
[39] G. Indiveri, E. Chicca, and R. Douglas, "A VLSI array of low-power spiking neurons and bistable synapses with spike-timing dependent plasticity," *IEEE Trans. Neural Netw.*, vol. 17, no. 1, pp. 211–221, Jan. 2006.
[40] P. E. Allen and D. R. Holberg, *CMOS Analog Circuit Design*, 2nd ed. Oxford, U.K.: Oxford Univ. Press, 2002.
[41] B. Razavi, *Design of Analog CMOS Integrated Circuits*. Boston, MA: McGraw-Hill, 2001.
[42] P. D. Roberts and C. C. Bell, "Spike timing dependent synaptic plasticity in biological systems," *Biol. Cybern.*, vol. 87, nos. 5–6, pp. 392–403, Dec. 2002.

Juan Huo received the B.Eng. degree from the Huazhong University of Science and Technology, Wuhan, China, in 2004, and the M.Sc. and Ph.D. degrees from the University of Edinburgh, Edinburgh, U.K., in 2006 and 2010, respectively. She studied in the Doctoral Training Center of informatics school and engineering school in different time periods.

She is currently an Assistant Professor with Shanghai Jiaotong University, Shanghai, China, and Zhengzhou University, Zhengzhou, China. Her current research interests include informatics, neural computation to electronics engineering.

Alan Murray (M'91–SM'93–F'07) is a Professor of neural electronics and the Head of the School of Engineering, University of Edinburgh, Edinburgh, U.K. He introduced the pulse stream method for analogue neural VLSI in 1985. He has published over 300 academic papers. His current research interests include biologically inspired computational forms, particularly in VLSI hardwares, where noise and overt temporal behavior are important, and direct interaction between silicon and real neuronal cells and networks.

Prof. Murray is a fellow of HEA, IET, and the Royal Society of Edinburgh.

Dongqing Wei is the Acting Head with the Department of Bioinformatics and Biostatistics, College of Life Science and Biotechnology, Shanghai Jiaotong University, Shanghai, China. His current research interests include bioinformatics and computer aided drug designs.

Dr. Wei is a member of the State Key Laboratory of Microbial Metabolism, the Editor-in-Chief of Interdisciplinary Sciences-Computational Life Sciences, and an Editorial Board Member of 13 international journals.